AAS 23-153

ADVANCED MODELING OF CONTROL-STRUCTURE INTERACTION IN THRUST VECTOR CONTROL SYSTEMS

Jeb S. Orr[*], Timothy M. Barrows[†], Colter W. Russell[‡], Richard K. Moore[§], Abran Alaniz[¶], and Stephen G. Ryan[‖]

The Space Launch System (SLS) Core Stage (CS) Thrust Vector Control (TVC) system is comprised of 8 mechanical feedback Shuttle heritage Type III TVC actuators and four RS-25 engines, each attached to a Shuttle heritage gimbal block/bearing. Two actuators are used to move each engine in two planes perpendicular to one another (i.e., pitch and yaw). The TVC system design leverages hardware from the Space Shuttle program as well as new hardware designed specifically for the Core Stage.

During the development of the SLS TVC system, a family of advanced dynamics models were developed to extend and compliment the simplified quasi-linear "simplex" model historically used for flight control design and stability analysis. The importance of these advanced models became increasingly evident after ambient and hot fire testing of the Core Stage, which revealed a number of findings associated with the dynamic response of the TVC integrated system. Test responses suggested that the TVC did not meet its performance specifications and its step and frequency responses exhibited unexpected departures from prior lab tests and modeled behavior. One driving factor for these results was a higher-than-expected degree of coupling between the TVC system, the engine dynamics, and the Core Stage structure.

This paper is the third installment in a seven-paper series surveying the design, engineering, test validation, and flight performance of the Core Stage Thrust Vector Control system. In this paper, a new method of modeling rocket vehicle thrust vectoring servoelastic dynamics is presented. In this approach, the load dynamics are replaced by a detailed finite element model containing both the rigid body and elastic modes. A partitioning technique is used to compute the effective compliance from the modal data and obtain accurate simulation results using a reduced number of generalized coordinates. Coupled backup structure and nozzle attach compliance effects on multiple engines are captured in higher fidelity than with a spring approximation, eliciting novel effects due to the complex load paths involved in the Core Stage structure. Validation of the model is demonstrated using a variety of structural/modal, laboratory, and full-scale hot fire test data.

1 INTRODUCTION

In the aerospace domain, it is important to develop accurate models of servoactuator systems to support the design of flight control algorithms. More so than in many applications, in launch vehicles having gimbaled engines, the contributions of the thrust loading and inertial coupling effects of

[*]Space Launch System Flight Dynamics and Control Technical Specialist (Mclaurin Aerospace / ESSCA), Knoxville, TN
[†]Principal Member of the Technical Staff, Draper (Retired), Cambridge, MA
[‡]Flight Systems Technical Staff, Mclaurin Aerospace (Jacobs ESSCA), Knoxville, TN
[§]Flight Systems Principal Staff, Mclaurin Aerospace (Jacobs ESSCA), Seattle, WA
[¶]Flight Systems Principal Staff, Mclaurin Aerospace (Jacobs ESSCA), Houston, TX
[‖]SLS Chief Engineer's Office (MTS CPSS), Huntsville, AL

the articulated engine nozzles can significantly influence the structural dynamic response. The goal of a thrust vector control (TVC) actuator model is to accurately reproduce the dynamic response of the engine and thrust vector to both flight software commands and external load torques. Such a model can be combined with test data to produce a validated representation of the engine-actuator system, used to verify requirements. Thereafter, a simplified model can be synthesized for integration with a high-fidelity linear or nonlinear model of the vehicle dynamics. This fully integrated simulation is then used to determine flight control gains and filters and verify the stability of the integrated engine-vehicle system prior to flight.

The Space Launch System (SLS) hydraulic actuator (Figure 1) is a pressure-stabilized, three-stage, quad-redundant position control system, originally developed and qualified for use with the RS-25D Space Shuttle Main Engine (SSME) and adapted to control the RS-25E Core Stage Engine (CSE) used on the Space Launch System launch vehicle.[3,4] This actuator contains a servovalve package with 4 current-controlled servovalves driven by an external TVC Actuator Controller (TAC). However, the servoloop feedback is entirely mechanical and no power other than hydraulic pressure is required to operate the actuator. Piston feedback is provided via a roller cam assembly that provides nulling torques on all four servovalves while load damping is provided by a passive hydraulic pressure feedback (DPF) assembly. Current inputs to the servovalve torque motors apply a bias which induces flow until the servovalve torque is equalized by the piston position feedback cam. As such, piston position is directly proportional to input current. With its exceptional design and precision tolerances, the SLS actuator is able to achieve a reasonably linear response over an impressive range of loading conditions and control piston displacements.

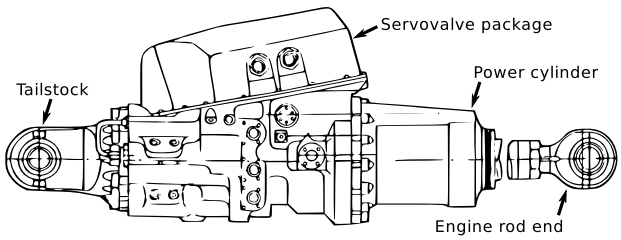

Figure 1. Typical SLS Hydraulic Actuator

In the NASA launch vehicle community, TVC models traditionally used for design verification fall into two categories: a high-fidelity, nonlinear ("complex") model, and a lower-fidelity, linearized or mostly-linear ("simplex") model. In the case of a hydraulic actuator, the former represents all of the internal nonlinearities and flow limitations, and is valid over a wide range of command amplitudes and operating conditions. Such models are used in detailed functional requirements verification, i.e., in a software-in-the-loop (SIL) simulation environment. The simplex model is a simplified representation of the complex model, valid for small signals and used for linear stability analysis of the flight control system.

During the development of the Space Launch System Core Stage TVC system, additional fidelity was required to represent the predicted (and later observed) response of the TVC system in flight or flight-like boundary conditions, as seen during the Green Run ambient and hot fire vectoring tests conducted in the Stennis Space Center B-2 test stand in January and March of 2021 (Figure 2). The notable discrepancy between modeling and test, particularly in the non-firing case, was an observed change in the apparent load resonance frequency of the engine-structure-actuator sys-

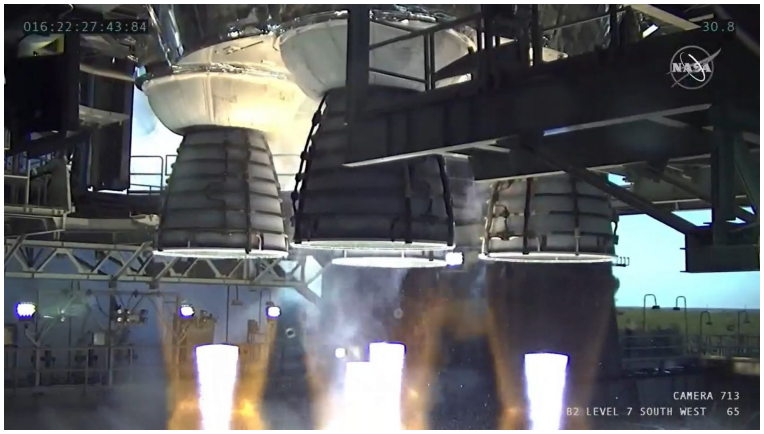

Figure 2. SLS Green Run Hot Fire Test #1, SSC B-2, January 16, 2021 ***(NASA TV)***

tem. In non-firing conditions, this resonance depends almost entirely on the compliance of the stage backup structure and engine attach load path. While it was not surprising that the actual structural compliance was higher than predicted by the design, it was determined that the single-spring approximation traditionally used in the planar, single-DoF simplex model could be improved upon by directly incorporating information about the structure from a finite element model (FEM).

As of the Green Run hot fire test, NASA MSFC's Multiple Actuator Stage Vectoring (MASV) simulation model had already undergone development to support verification of the servoelastic stability of the TVC system coupled to the core stage structure. Since high-power actuation systems must actively stabilize the load, MASV was used to verify that all eight actuator degrees of freedom were robustly stable with respect to the elastic modes of the core stage structure, as reflected into the actuator position feedback loop.

The MASV model is a mechanism whereby the traditional single-DoF simplex model is extended to incorporate a modal representation of the rigid and elastic DoFs of multiple engines, coupled with multiple actuators in flight-like boundary conditions. In the case of the SLS Core Stage, this includes four engines, eight actuators, and many thousands of degrees of freedom as represented in a high-fidelity FEM. The MASV implementation has been successfully verified using an independently-developed, generalized elastic multibody simulation (DARTS/DSHELL).[1,2]

MASV is used to support test validation of the SLS Core Stage TVC parameters, including those derived from finite element model data, by correlating the fully-coupled response of the engine-structural system to ground test data in both ambient and static firing conditions. While not representative of all of the nonlinearities that affect the TVC system response (particularly friction), MASV has the highest-fidelity representation of the structural dynamics and the associated load paths and was part of the overall toolchain used for development of the Artemis I mission flight rationale.[8] The derivation and development of MASV is the topic of the present paper. Further analysis as applied to the SLS Core Stage and model correlation performed using MASV are discussed further in the companion papers.[6,7]

1.1 Traditional Model

The simplex model is a compact representation of the TVC system containing only a few states, and is valid over a typical range of operating conditions. Typical simplifications in the hydraulic case

include the removal or linearization of nonlinearities in the small-signal regime, removal of kinematics and external pressure equalization dynamics, and consolidation of redundant servovalves and flow paths into a single transfer-function representation. These models are used in linear stability analysis to assess the effects of flight control stability, global servoelasticity, and so on. Due to the dependence of the inertial coupling ("tail-wag-dog" or TWD) effect on the engine acceleration, the simplest model that provides an appropriate representation of the open-loop phase lag and TWD effects has three states: two states for the engine angle and angular rate, and a third state representing the actuator lag, e.g., the hydraulic power cylinder.

In practice, the model must also account for the servovalve dynamics, pressure feedback, and the compliance of the load, so a typical linear model has six states. Since the oil and structure are both compliant at high loads, the position of the piston and that of the load (the engine) differ. The actuator's integrating position feedback eliminates the effect of the oil and actuator structural compliances between the actuator endpoints, and actively stabilizes the load resonance of the engine combined with the backup structure. Dynamic pressure feedback (DPF) adds damping to the load resonance, and provides a remarkably well-damped response with good phase lead characteristics near the rigid-body control frequency.

This combination of active stabilization and load feedback also has the important feature that tends to improve flight control stability margins for global modes that have a strong coupling with the aft structure of the launch vehicle. That is, the actuators indirectly act as active dampers for certain servoelastic interactions. Such effects are uncovered using a high-fidelity vehicle-level servoelastic coupling model.[9] (Conversely, thrust vector servoelasticity can be destabilizing, as in the case of the SLS booster antisymmetric bending, but was found to be inconsequential in the presence of elastic jet damping effects).

In a simplex model, it is typical to represent the compliance of the load by combining the engine and stage compliances into a single spring. While this assumption is warranted in most cases, strong coupling with secondary modes other than the fundamental load resonance requires careful verification that these modes do not present a servoelastic concern. More importantly, a value of this load spring must be determined, and it can usually only be ascertained from a test-validated model.

1.2 Multiple Actuator Stage Vectoring (MASV) Model

The MASV formulation is intended to complement the vehicle-level reduced-body approach for coupling the engine-servo dynamics and the vehicle global bending modes. Importantly, this approach can be used to demonstrate that the local compliance effects, typically several decades above the global vehicle bending modes, can be omitted from the global vehicle model if their effect on servoloop response is shown to be negligible (as intended in the servoloop design).

The structure of the paper is as follows. In Section 2, a review of the simplex model formulation is presented, and a state model is derived assuming a single-spring approximation of the load and a rigid engine. In Section 3, the rigid load is replaced with a modal representation. In Section 4, it is shown that a portion of the structural modes from the finite element model can be collapsed into a static compliance without a significant loss of fidelity. In Section 5, the use of MASV to support TVC performance validation using both ambient and static firing data is discussed.

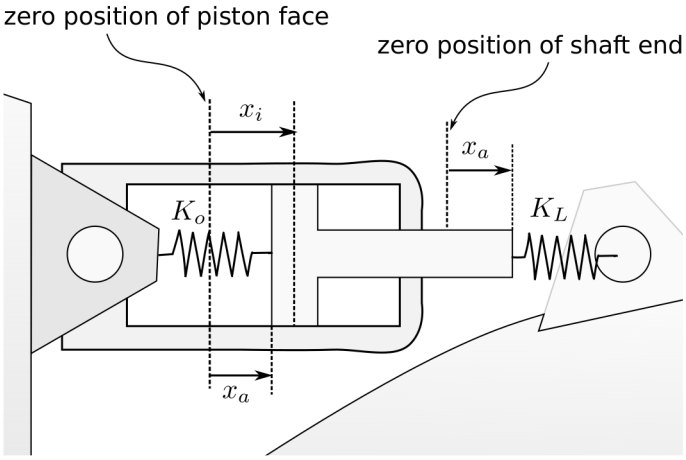

Figure 3. TVC actuator with load compliance

2 SIMPLEX MODEL

Consider the notional diagram of a hydraulic actuator given in Figure 3. In this simplified model, the actuator components are massless and the only compliances are in the load K_L and the hydraulic oil K_o.* The load compliance is a single spring that represents all of the compliance in the system, including the actuator components outside the position control loop, the engine structure, and the backup structure.

The total compliance from the rocket stage to the (rigid) engine interface is

$$K_T = \left(\frac{1}{K_L} + \frac{1}{K_o} \right)^{-1} \tag{1}$$

and the linear displacement of the rigid engine is given by

$$x_E = R\beta \tag{2}$$

where R is the equivalent moment arm calculated about the actuator null position and β is the engine angular displacement (in radians). It is helpful to introduce the ideal piston position x_i which can be thought of as the displacement of the piston if the oil were not compressible. The ideal piston position is related to the flow by

$$\dot{x}_i = \frac{1}{A_p} Q \tag{3}$$

where A_p is the piston area and Q is the input flow. For small signals, the dynamics of the spool and servovalves at the input of the power cylinder are well-represented by a second-order linear system of the form

$$H(s) = \frac{Q(s)}{u(s)} = \frac{k_v \omega_v^2}{s^2 + 2\zeta_v \omega_v s + \omega_v^2} \tag{4}$$

*In this discussion, it is assumed that the compliance of the oil, which depends strongly on fluid air entrainment, is the most significant factor affecting the total compliance within in the servo position loop. The structural compliance of the actuator body and the radial elasticity of the cylinder also contribute to the actuator compliance, but are generally much less than that of the oil. In practice, these effects are combined to form a single actuator stiffness K_{ac}.

where u and Q are the servovalve torque input and output flow rate, k_v is the valve package gain, and $\zeta_v,\ \omega_v$ are the damping and natural frequency, respectively.

The actual displacement of the piston x_a is less than x_i due to the compliance of the oil and the actuator body. The displacement of the engine, x_E, is less than x_a due to the fact that K_L is not infinite. Thus we can write

$$x_E = x_a - \frac{f_a}{K_L} \tag{5}$$

where

$$f_a = K_T \left(x_i - x_E \right) \tag{6}$$

is the force developed in the actuator. Combining these expressions,

$$x_a = \left(1 - \frac{K_T}{K_L} \right) R\beta + \frac{K_T}{K_L} x_i. \tag{7}$$

The engine dynamics can be written as

$$J_n \ddot{\beta} = f_a R - C_n \dot{\beta} - K_n \beta$$

where the first term on the right-hand side of the equation is the actuator torque on the rigid engine. The damping coefficient C_n is a viscous damping approximation to dissipation in the load dynamics, and the angular stiffness K_n represents gravitational restoring torque and loads about the engine gimbal due to the pressurized propellant feedlines. Substituting from (6) and then from (2) it follows that

$$J_n \ddot{\beta} = K_T R x_i - C_n \dot{\beta} - \left(K_n + K_T R^2 \right) \beta \tag{8}$$

The engine natural frequency for a stationary actuator ($x_i = 0$) with zero damping is

$$\omega_p = \sqrt{\frac{K_T R^2 + K_n}{J_n}}. \tag{9}$$

This is called the *pendulum mode* frequency. It represents the natural frequency of the engine-structure-actuator system when the compliance of the structure and oil is included and the actuator is inoperative. Compared with the effect of the structure, the contribution of K_n in this equation, at $1g$, can be neglected for most liquid engines. (For SRMs, K_n can be much more significant due to the effects of a flex bearing).

Similarly, the *load resonance* frequency is

$$\omega_L = \sqrt{\frac{K_L R^2 + K_n}{J_n}}, \tag{10}$$

which depends only on the load compliance, and does not include the oil. As discussed in the companion papers,[6,8] the load resonance frequency appears as an antiresonance (notch) in the transfer function relating the piston position x_a to the servovalve input torque. This relationship is crucial for test-based validation of the load stiffness K_L, assuming that the moment arm and inertia can be determined separately. This fact was noted by Thompson[10] in the development of the simplex model.

In order to control the position of the load, a feedback mechanism is used to sense the displacement and the force. Since the direct sensing of the engine position is not feasible, a piston position measurement (Equation 7) is determined via the actuator's internal mechanical feedback cam. The second component, the load feedback, depends on the differential pressure ΔP developed in the actuator. The differential pressure ΔP is equal to the actuator force (Equation 6) divided by the piston area;

$$\Delta P = \frac{1}{A_p} f_a. \tag{11}$$

Load feedback is used to add damping to the load; i.e., the engine-structural resonance, which becomes proportional to the load velocity after integration by the power cylinder. Since direct load feedback would produce an unacceptable steady-state error, the load feedback is filtered using a hydraulic high-pass filter, which has the dynamics

$$\dot{z}_d = -\frac{1}{\tau_p} z_p + \Delta P. \tag{12}$$

This scheme is referred to as Dynamic Pressure Feedback (DPF). The quantity z_p is the state of the load feedback filter, and the output that is used for feedback is the state derivative $\dot{z}_p$. The value τ_p is the time constant associated with the load feedback dynamics. Combining (2), (12), and (11) gives the equation for the pressure feedback filter;

$$\dot{z}_p = -\frac{1}{\tau_p} z_p + \frac{1}{A_p} K_T \left(x_i - R\beta \right). \tag{13}$$

The engine slew control is performed by modulating the flow Q using both piston position feedback and pressure feedback. An external motor torque is applied to the servovalve that biases the equilibrium point obtained by mechanical feedback. The total servovalve torque input is given by

$$u = k_{tm} i_c - k_{fb} x_a - k_d \dot{z}_d \tag{14}$$

where x_a is the mechanical displacement across the actuator body and k_d is the DPF gain. The torque applied to the servovalve is proportional to the input current i_c. Using the load feedback and measured piston position expressions (6) and (7) to replace f_a and x_a with quantities related to the engine angle β, and substituting the state derivative $\dot{z}_d$ in Equation 14, the final set of simplex equations are given by

$$\dot{x}_i = \frac{1}{A_p} Q \tag{15}$$

$$\dot{z}_d = -\frac{1}{\tau_d} z_d + \frac{1}{A_p} K_T \left(x_i - R\beta \right) \tag{16}$$

$$\ddot{\beta} = \frac{K_T R}{J_n} x_i - \frac{C_n}{J_n} \dot{\beta} - \frac{K_n + K_T R^2}{J_n} \beta \tag{17}$$

along with the servo dynamics

$$\dot{Q} = z_v \tag{18}$$

and

$$\dot{z}_v = -2\zeta_v\omega_v z_v - \omega_v^2 Q + \left(k_v\omega_v^2 k_d \frac{1}{\tau_d}\right) z_d - \left(k_v\omega_v^2 K_T\left(\frac{k_d}{A_p} + \frac{k_{fb}}{K_L}\right)\right) x_i$$
$$+ k_v\omega_v^2 R\left(\frac{k_d}{A_p}K_T - k_{fb}\left(1 - \frac{K_T}{K_L}\right)\right)\beta + k_v\omega_v^2 k_{tm} i_c. \quad (19)$$

This model can be mechanized in a state model form $\dot{\mathbf{x}} = \mathbf{A}\mathbf{x} + \mathbf{b}i_c$, $\mathbf{y} = \mathbf{C}\mathbf{x}$ using the state vector

$$\mathbf{x} = \begin{bmatrix} x_i & z_d & Q & z_v & \beta & \dot{\beta} \end{bmatrix}^T \quad (20)$$

and the system matrices

$$\mathbf{A} = \begin{bmatrix} 0 & 0 & \frac{1}{A_p} & 0 & 0 & 0 \\ \frac{1}{A_p}K_T & -\frac{1}{\tau_d} & 0 & 0 & -\frac{1}{A_p}K_T R & 0 \\ 0 & 0 & 0 & 1 & 0 & 0 \\ -k_v\omega_v^2 K_T\left(\frac{k_d}{A_p} + \frac{k_{fb}}{K_L}\right) & \frac{k_v\omega_v^2 k_d}{\tau_d} & -\omega_v^2 & -2\zeta_v\omega_v & k_v\omega_v^2 R\left(\frac{k_d}{A_p}K_T - k_{fb}\left(1 - \frac{K_T}{K_L}\right)\right) & 0 \\ 0 & 0 & 0 & 0 & 0 & 1 \\ \frac{K_T R}{J_n} & 0 & 0 & 0 & -\frac{\left(K_n + K_T R^2\right)}{J_n} & -\frac{D_n}{J_n} \end{bmatrix}$$

$$\mathbf{b} = \begin{bmatrix} 0 \\ 0 \\ 0 \\ k_v\omega_v^2 k_{tm} \\ 0 \\ 0 \end{bmatrix} \quad (21)$$

The outputs are the engine angle and actuator piston position

$$\mathbf{y} = \begin{bmatrix} \beta \\ x_a \end{bmatrix} \quad (22)$$

The engine angle β can be taken directly from the state vector; the actual piston position is given by Equation 7 and therefore

$$\mathbf{C} = \begin{bmatrix} 0 & 0 & 0 & 0 & 1 & 0 \\ \frac{K_T}{K_L} & 0 & 0 & 0 & R\left(1 - \frac{K_T}{K_L}\right) & 0 \end{bmatrix}. \quad (23)$$

3 MODAL MODEL

Incorporating a modal model of the structure with the actuator dynamics allows the load path to be represented, hypothetically, by a structural model of arbitrary fidelity. A modal representation allows an analyst to isolate the modal components that contribute most significantly to the response and identify physical characteristics of the structure that influence the servodynamic response.

Suppose the engine degrees of freedom are described by a FEM with K orthogonal modes instead of a rigid-body engine model (Figure 4). Associated with this FEM are the gridpoints at the two

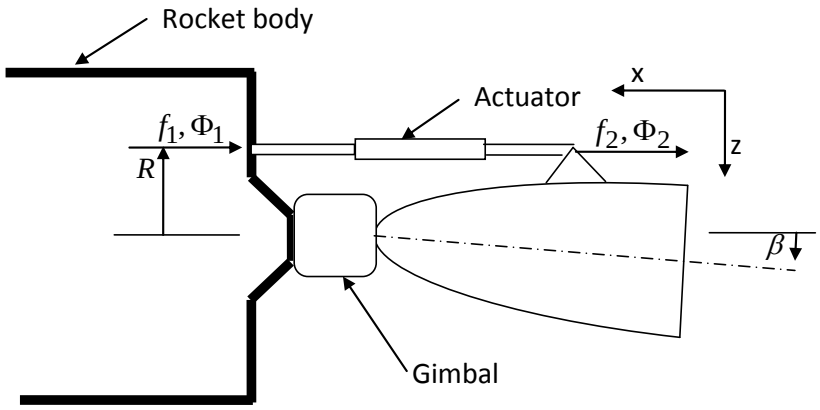

Figure 4. Rocket Nozzle and Coordinate Frame

attach points of the actuator. The bending equation in generalized coordinates is given by

$$\ddot{\boldsymbol{\eta}} + \mathbf{D}\dot{\boldsymbol{\eta}} + \boldsymbol{\Omega}^2\boldsymbol{\eta} = \boldsymbol{\Phi}_1^T\mathbf{f}_1 + \boldsymbol{\Phi}_2^T\mathbf{f}_2 + \boldsymbol{\Psi}_\beta^T\left(\mathbf{g}_s + \mathbf{g}_d\right) + \boldsymbol{\Phi}_0^T\mathbf{f}_0 \tag{24}$$

where $\mathbf{D}$ is a viscous damping matrix, $\boldsymbol{\Omega}^2 = \mathrm{diag}(\omega_i^2)$, $\mathbf{f}_j$ is the applied force at each attach point, and $\mathbf{g}_s$, $\mathbf{g}_d$ are the spring and damping torques applied at the gimbal point, respectively. The engine angle is described by

$$\boldsymbol{\beta} = \left(\boldsymbol{\Psi}_\beta - \boldsymbol{\Psi}_0\right)\boldsymbol{\eta} = \tilde{\boldsymbol{\Psi}}_\beta\boldsymbol{\eta} \tag{25}$$

where $\boldsymbol{\beta} \in \mathbb{R}^3$ is, in general, a three-axis small rotation about the nominal engine position, and $\boldsymbol{\Psi}_\beta \in \mathbb{R}^{3\times K}$ is the mode slope on the rotating side of the engine gimbal. The external thrust load $\mathbf{f}_0$ is applied at the gimbal interface, where $\boldsymbol{\Phi}_0 \in \mathbb{R}^{3\times K}$ is the mode shape on the fixed (thrust structure) side.

For a freely rotating (frictionless) gimbal, this point must be unconstrained in the FEM so that the engine is free to pivot. Likewise, the quantity $\boldsymbol{\Psi}_0$ is the mode slope on the fixed side of the gimbal, or at some point in the thrust structure that corresponds to the local control actuation plane. Thus, $\boldsymbol{\beta}$ represents the rotation of the engine structure with respect to the thrust structure, which is the controlled quantity as represented in the simplex model. It is important to distinguish between this quantity and

$$\boldsymbol{\beta}_g = \boldsymbol{\Psi}_\beta\boldsymbol{\eta} \tag{26}$$

which is the rotation of the engine structure with respect to the *global* undeformed vehicle coordinate system. Since, in general, the addition of external thrust loads, dynamic response, and varying boundary conditions may cause differing degrees of thrust structure deformation, $\boldsymbol{\beta}_g \neq \boldsymbol{\beta}$, in general.

The spring and damping torques are given by

$$\mathbf{g}_s = -\mathbf{K}_n\boldsymbol{\beta} + m_n\mathbf{g}_0^{\times}\mathbf{r}_n^{\times}\boldsymbol{\beta}_g = -\left(\mathbf{K}_n\tilde{\boldsymbol{\Psi}}_\beta - m_n\mathbf{g}_0^{\times}\mathbf{r}_n^{\times}\boldsymbol{\Psi}_\beta\right)\boldsymbol{\eta} \tag{27}$$

$$\mathbf{g}_d = -\mathbf{D}_n\dot{\boldsymbol{\beta}} = -\mathbf{D}_n\tilde{\boldsymbol{\Psi}}_\beta\dot{\boldsymbol{\eta}} \tag{28}$$

where the nozzle mass m_n and center of mass location $\mathbf{r}_n$ affect the gravitational load torque. The gravitational stiffening has been separated from the usual nozzle angular stiffness term, since it must be computed with respect to the global frame. It is also important to distinguish between $\mathbf{D}_n$, representing the damping torque applied at the gimbal point, and the matrix $\mathbf{D}$ representing the modal damping. For liquid engines, the term $\mathbf{D}_n$ can approximate the friction of the gimbal bearing and account for any residual velocity-dependent damping as measured via test. For conservatism, $\mathbf{D}$ is usually chosen as a diagonal viscous damping matrix with $\zeta_i = 0.005$, but Rayleigh damping has also been shown to compare favorably with test.

It is assumed in the present discussion that these auxiliary stiffness and damping matrices are diagonal and have no axial components; however, this need not be the case. In the case of the RS-25 engine, the feedline torques are not symmetric about the gimbal axis. Compared with the backup structure stiffness and actuator forces, however, they are too small to measure to any degree of confidence. Other real effects, particularly compliance of the gimbal attach structure, may lead to a non-diagonal auxiliary stiffness matrix. These values can be estimated via detailed modeling and validated through testing.

If the test structure is vertical, the external load $\mathbf{f}_0$ is equal to

$$\mathbf{f}_0 = (\mathbf{I} + \boldsymbol{\beta}_g)\,\mathbf{u}_0 F_T - m_n\mathbf{g}_0 \tag{29}$$

$$= F_T\mathbf{u}_0 - m_n\mathbf{g}_0 - F_T\mathbf{u}_0^{\times}\boldsymbol{\Psi}_\beta\boldsymbol{\eta}. \tag{30}$$

where the nominal thrust unit vector is $\mathbf{u}_0$, and $m_n\mathbf{g}_0$ represents the weight of the engine. The first two terms are static and can be omitted from a linear analysis. The remaining term is the follower effect, and should be retained to capture the dependency of the thrust vector on the global engine angle.

It is assumed that for the present model and to be consistent with the linearization of the finite element model, deflections of the engine are small angles from the nominal (null) position of the engine. The actuator force is resolved along a unit vector $\mathbf{p}$ that points along the direction of the actuator line of action as used in the previous section. It is not necessary that the actuator be aligned in any particular way with the vehicle body frame; $\mathbf{p}$ is directly computed from the FEM geometry. The applied force vectors are related to the scalar actuator force by

$$\mathbf{f}_1 = -f_a\mathbf{p} \tag{31}$$

$$\mathbf{f}_2 = f_a\mathbf{p} \tag{32}$$

These forces excite the structure at the two points shown in Figure 4. For a single nozzle with two actuators, the FEM will contain two zero-frequency modes (rigid-body modes) that represent the equivalent of the nozzle deflections β_y and β_z. The remaining modes will represent the structural deflections. When all the modes are included, the FEM provides the total actuator output as given by Equation 25, and it is not necessary to distinguish between $R\beta$ and x_{str} . The actuator output equation can be replaced by the component of the net deflection in the direction of $\mathbf{p}$:

$$x_a = \mathbf{p}^T \left(\mathbf{\Phi}_2 - \mathbf{\Phi}_1 \right) \boldsymbol{\eta} \tag{33}$$

Defining

$$\boldsymbol{\gamma}^T = \mathbf{p}^T \left(\mathbf{\Phi}_2 - \mathbf{\Phi}_1 \right), \tag{34}$$

the quantity $\boldsymbol{\gamma}$ is the modal compliance coefficient. It is a constant derived from the finite element model geometry and its eigenvectors. The modal equation and actuator position equations can now be written as

$$\begin{aligned} \ddot{\boldsymbol{\eta}} + \mathbf{D}\dot{\boldsymbol{\eta}} + \mathbf{\Omega}^2 \boldsymbol{\eta} &= \left(\mathbf{\Phi}_1^T - \mathbf{\Phi}_2^T \right) \mathbf{p} f_a + \tilde{\mathbf{\Psi}}_\beta{}^T \left(\mathbf{g}_s + \mathbf{g}_d \right) + \mathbf{\Phi}_0^T \mathbf{f}_0 \\ &= \boldsymbol{\gamma} f_a + \tilde{\mathbf{\Psi}}_\beta{}^T \left(\mathbf{g}_s + \mathbf{g}_d \right) + \mathbf{\Phi}_0^T \mathbf{f}_0 \end{aligned} \tag{35}$$

$$x_a = \boldsymbol{\gamma}^T \boldsymbol{\eta} \tag{36}$$

The quantity

$$x_{ac} = x_i - x_a \tag{37}$$

can be used to describe the actuator compliance; that is, the displacement of the actuator due to the compliance of the oil and actuator structure. Note that the ideal actuator position x_i introduced in Equation 3 is not an actual displacement, but can be thought of as proportional to the time integral of the flow. The actuator force becomes

$$f_a = K_{ac} x_{ac} = K_{ac} \left(x_i - \boldsymbol{\gamma}^T \boldsymbol{\eta} \right) \tag{38}$$

Using this expression and Equations 25 through 28, and grouping terms, the elastic equation becomes

$$\ddot{\boldsymbol{\eta}} = \boldsymbol{\gamma} K_{ac} x_i - \left(\mathbf{D} + \tilde{\mathbf{\Psi}}_\beta^T \mathbf{D}_n \tilde{\mathbf{\Psi}}_\beta \right) \dot{\boldsymbol{\eta}} - \left(\mathbf{\Omega^2} + K_{ac} \boldsymbol{\gamma}\boldsymbol{\gamma}^T + \tilde{\mathbf{K}} \right) \boldsymbol{\eta} + \mathbf{\Phi}_0^T \left(F_T \mathbf{u}_0 - m_n \mathbf{g}_0 \right) \tag{39}$$

where

$$\tilde{\mathbf{K}} = \tilde{\mathbf{\Psi}}_\beta^T \left(\mathbf{K}_n \tilde{\mathbf{\Psi}}_\beta - m_n \mathbf{g}_0^\times \mathbf{r}_n^\times \mathbf{\Psi}_\beta \right) + F_T \mathbf{\Psi}_0{}^T \mathbf{u}_0^\times \mathbf{\Psi}_\beta .$$

Note that the term K_{ac} is equivalent to K_o as used in Section 2. It is straightforward to use Equation 39 to extend the analysis of Section 2 and incorporate the actuator dynamics (x_i). The state vector for the updated model can be chosen as

$$\mathbf{x} = \begin{bmatrix} x_i & z_d & Q & z_v & \boldsymbol{\eta} & \dot{\boldsymbol{\eta}} \end{bmatrix}^T \tag{40}$$

By inserting Equation 38 into Equation 16, the pressure feedback dynamics are given by

$$\dot{z}_d = -\frac{1}{\tau_d} z_d + \frac{K_{ac}}{A_p} \left(x_i - \boldsymbol{\gamma}^T \boldsymbol{\eta} \right) \tag{41}$$

By using Equations 36 and 41 to modify Equation 19, the servovalve feedback expression is given by

$$\dot{z}_v = -2\zeta_v\omega_v z_v - \omega_v^2 Q - \frac{k_v\omega_v^2 k_d}{\tau_d} z_d - \frac{k_v\omega_v^2 k_d K_{ac}}{A_p}\left(x_i - \boldsymbol{\gamma}^T\boldsymbol{\eta}\right) - k_v\omega_v^2 k_{fb}\boldsymbol{\gamma}^T\boldsymbol{\eta} + k_v\omega_v^2 k_{tm} i_c \quad (42)$$

In the generic form $\dot{\mathbf{x}} = \mathbf{A}\mathbf{x} + \mathbf{b}i_c$, omitting zero-order terms, the system matrices are

$$\mathbf{A} = \begin{bmatrix} 0 & 0 & \frac{1}{A_p} & 0 & \mathbf{0}_K^T & \mathbf{0}_K^T \\ \frac{K_{ac}}{A_p} & -\frac{1}{\tau_d} & 0 & 0 & -\frac{K_{ac}}{A_p}\boldsymbol{\gamma}^T & \mathbf{0}_K^T \\ 0 & 0 & 0 & 1 & \mathbf{0}_k^T & \mathbf{0}_K^T \\ -\frac{k_v\omega_v^2 k_d K_{ac}}{A_p} & \frac{k_v\omega_v^2 k_d}{\tau_d} & -\omega_v^2 & -2\zeta_v\omega_v & k_v\omega_v^2\left(\frac{k_d K_{ac}}{A_p} - k_{fb}\right)\boldsymbol{\gamma}^T & \mathbf{0}_K^T \\ \mathbf{0}_K & \mathbf{0}_K & \mathbf{0}_K & \mathbf{0}_K & \mathbf{0}_{K\times K} & \mathbf{1}_{K\times K} \\ K_{ac}\boldsymbol{\gamma} & \mathbf{0}_K & \mathbf{0}_K & \mathbf{0}_K & -\left(\boldsymbol{\Omega}^2 + K_{ac}\boldsymbol{\gamma}\boldsymbol{\gamma}^T + \tilde{\mathbf{K}}\right) & -\left(\mathbf{D} + \tilde{\boldsymbol{\Psi}}_\beta^T\mathbf{D}_n\tilde{\boldsymbol{\Psi}}_\beta\right) \end{bmatrix}$$

$$\mathbf{b} = \begin{bmatrix} 0 \\ 0 \\ 0 \\ k_v\omega_v^2 k_{tm} \\ \mathbf{0}_K \\ \mathbf{0}_K \end{bmatrix}. \quad (43)$$

Here $\mathbf{0}_K$ is a null vector with *K* elements, $\mathbf{0}_{K\times K}$ is a square null matrix of dimension K, and $\mathbf{1}_{K\times K}$ is an identity matrix of dimension K. This model is valid for a single actuator and an arbitrary number of engine degrees of freedom. In the MASV implementation, this structure is block-diagonalized with a single set of elastic modes to represent multiple actuators and engines.

4 STATIC AND DYNAMIC MODES

The previous section assumes that the modes from the FEM can be used to represent all of the deflection that results from an actuator force. Although this is possible in theory, in practice it becomes necessary to include a very large number of modes from the FEM in order to fully capture the displacements and accelerations of the attach points at the nozzle and backup structure. The present section introduces a method whereby the full compliance can be approximated using a only a small number of modes.

In this technique, a frequency cutoff is defined, such that only those modes that are below this frequency are included in the state-space model. This set of modes is referred to as the *dynamic* modes. The modes that are not included, i.e., those that are above the cutoff, are *static* modes. To analyze these static modes, we begin with the elastic equation, neglecting the spring and damping torques $\mathbf{g}_s$, $\mathbf{g}_d$ and external loads that are applied at the gimbal.

$$\ddot{\boldsymbol{\eta}} + \mathbf{D}\dot{\boldsymbol{\eta}} + \boldsymbol{\Omega}^2\boldsymbol{\eta} = \left(\boldsymbol{\Phi}_1^T - \boldsymbol{\Phi}_2^T\right)\mathbf{p}f_a = \boldsymbol{\gamma}f_a \quad (44)$$

In its modal representation, the system dynamics are uncoupled (diagonal), and therefore each scalar equation appears in the form

$$\ddot{\eta}_k + D_k\dot{\eta}_k + \Omega_k^2\eta_k = \gamma_k f_a \tag{45}$$

Here, k represents the mode number.

The choice of cutoff frequency is based on the assumption that for modal frequencies $\Omega_k \gg \omega_L$, that is, much greater than the load resonance frequency, the settling time of the structural dynamics is such that $\ddot{\eta}_k \approx 0$ on a much faster timescale than that of the actuator dynamics. If this is the case, the modal displacement is directly proportional to the applied force;

$$\eta_k \approx \frac{\gamma_k f_a}{\Omega_k^2}, \qquad k > J \tag{46}$$

In this expression, it is assumed that the modes are sorted by frequency, and that J is the number of the highest frequency mode to be included in the dynamics. For the static modes, in scalar form, Equation 36 is written

$$x_a = \sum \gamma_k \eta_k, \tag{47}$$

which is composed of the sum of the effective engine displacement (x_E) and the structural displacement. The structural displacement contains both a dynamic component x_d and static component x_s;

$$x_a = x_E + x_d + x_s \tag{48}$$

In the simple case of one engine with two actuators and a FEM constrained to have only two free DoF about the gimbal, there will be two rigid-body modes. The effective displacement can be written as

$$x_E = \gamma_1\eta_1 + \gamma_2\eta_2. \tag{49}$$

Here, η_1 and η_2 correspond to the modes whose eigenvalues in the generalized stiffness matrix are equal to zero.

The static and dynamic displacements are given by

$$x_s = \sum_{k=J+1}^{K} \gamma_k\eta_k \approx \sum_{k=J+1}^{K} \frac{\gamma_k^2 f_a}{\Omega_k^2} \tag{50}$$

$$x_d = \sum_{k=3}^{J} \gamma_k\eta_k \tag{51}$$

The load compliance can then be defined as

$$C_s = \frac{x_s}{f_a} = \sum_{i=J+1}^{K} \frac{\gamma_k^2}{\Omega_k^2}. \tag{52}$$

The inverse of this quantity is K_s, which is analogous to the load stiffness in Equation 1. It is emphasized that this static load stiffness is only a portion of the total load stiffness, because the remaining dynamics are represented using lower-frequency modes from the finite element model.

In the equations of motion, overbars are used to designate the following vectors in which the static modes have been removed via truncation;

$$\bar{\boldsymbol{\gamma}} = \begin{bmatrix} \gamma_1 & \gamma_2 & \cdots & \gamma_J \end{bmatrix}^T \tag{53}$$

$$\bar{\boldsymbol{\eta}} = \begin{bmatrix} \eta_1 & \eta_2 & \cdots & \eta_J \end{bmatrix}^T \tag{54}$$

The actuator displacement expression can then be partitioned as

$$x_a = \bar{\boldsymbol{\gamma}}^T \bar{\boldsymbol{\eta}} + f_a C_s \tag{55}$$

The actuator force in Equation 38 can be replaced with a partitioned version;

$$f_a = K_{ac} \left(x_i - \bar{\boldsymbol{\gamma}}^T \bar{\boldsymbol{\eta}} - f_a C_s \right). \tag{56}$$

This equation can be solved for the total actuator force f_a,

$$f_a = K_0 \left(x_i - \bar{\boldsymbol{\gamma}}^T \bar{\boldsymbol{\eta}} \right) \tag{57}$$

where

$$K_0 = \left(\frac{1}{K_s} + \frac{1}{K_{ac}} \right)^{-1}. \tag{58}$$

Equation 57 can be used to incorporate the static stiffness using overbarred variables and substituting K_0 for K_{ac} . Note that if J is chosen to incorporate only rigid-body modes, and a very large number of modes is included in calculating the static modes, $K_s \rightarrow K_L$ and $K_0 \rightarrow K_T$, the simplex approximations to the load stiffness and total stiffness, respectively. That is, the simplex model corresponds to the case in which all of the flexibility, except the rigid-body mode, is treated as static modes. A side effect of this relationship is that Equation 52 can be used to interrogate the FEM and determine an estimate of the load stiffness.

With the partitioning included, the final form of the elastic equation becomes

$$\ddot{\bar{\eta}} = \bar{\boldsymbol{\gamma}} K_0 x_i - \left(\mathbf{D} + \tilde{\boldsymbol{\Psi}}_\beta^T \mathbf{D}_n \tilde{\boldsymbol{\Psi}}_\beta \right) \dot{\bar{\boldsymbol{\eta}}} - \left(\boldsymbol{\Omega}^2 + \tilde{K}_T \bar{\boldsymbol{\gamma}} \bar{\boldsymbol{\gamma}}^T + \tilde{\mathbf{K}} \right) \bar{\boldsymbol{\eta}} + \boldsymbol{\Phi}_0^T \left(F_T \mathbf{u}_0 - m_n \mathbf{g}_0 \right) \tag{59}$$

Here, it is understood that all of the boldfaced parameters must be truncated to match the size of the overbarred quantities.

When there is no truncation of the modes, the 3-vector of nozzle angles (a small rotation) is obtained from Equation 25, in which $\tilde{\boldsymbol{\Psi}}_\beta$ is full-sized. With truncation, this expression can be written as

$$\boldsymbol{\beta} = \tilde{\boldsymbol{\Psi}}_\beta \bar{\boldsymbol{\eta}} + \sum_{k=J+1}^{K} \tilde{\boldsymbol{\psi}}_{\beta k} \eta_k \tag{60}$$

where the mode slope matrices $\boldsymbol{\Psi}$ are truncated accordingly to be consistent with Equation 59. This expression can be rewritten using Equations 46 and 57 such that

$$\boldsymbol{\beta} = \tilde{\boldsymbol{\Psi}}_{\beta}\bar{\boldsymbol{\eta}} + K_0\left(x_i - \bar{\boldsymbol{\gamma}}^T\bar{\boldsymbol{\eta}}\right)\sum_{k=J+1}^{K}\tilde{\boldsymbol{\psi}}_{\beta k}\frac{\gamma_k}{\Omega_k^2} \tag{61}$$

Note that the summation is a fixed parameter that only has to be computed once. It is entirely reasonable to select a very large number for K, which could represent as many as several thousand degrees of freedom.

5 RESULTS

As employed on the Space Launch System program, the present approach has been used for a variety of detailed analyses of control-structure interaction, as represented by a detailed finite element model that reproduces the boundary conditions of the core stage as installed in the B-2 test stand at SSC, or in flight.

A principal goal of these analyses was to determine the effect of higher-frequency modal content on the servoloop stability. A representative comparison between the open-loop Nichols (log-magnitude frequency response) of one actuator degree of freedom in both static conditions and with a modal representation is shown in Figure 5. The response shown on the left includes only rigid-body degrees of freedom: the modal representation of the engine consists only of the eight unconstrained engine DoF representing pitch and yaw rotations about each gimbal point. The remaining DoF (over 6,000 modes, including residual vectors) have been used to compute a static stiffness approximation according to Equation 52.

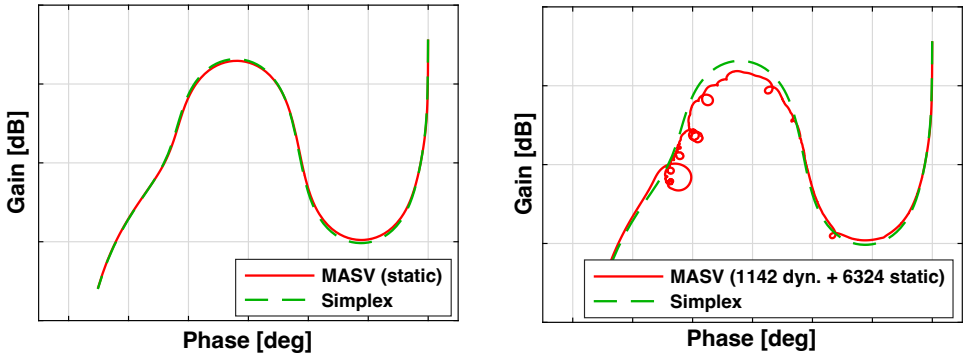

Figure 5. MASV core stage actuator servo loop break, GRHF configuration. Static approximation (left); dynamic modes to 25 Hz (right)

The dynamic model (Figure 5, right) represents the same configuration but with dynamic content truncated above 25 Hz. The modal representation (here, using about 1,000 dynamic modes) reproduces the spring load resonance in higher fidelity. In Figure 5, the simplex model with a rigid engine is shown for comparison (dashed lines). The rigid-body response is identical, although the MASV solution exhibits slightly higher damping. In the modal representation, the coupling of the elastic modes through the actuators effectively distributes dissipation across multiple modes, resulting in a resonance that is less concentrated at a single frequency.[†]

[†]This results in an effective coupled system damping matrix that is no longer diagonal.

As can be seen, the servoloop provides ample stability margin for variable load resonances in both gain, phase, and frequency. In fact, the range of load resonances that can be tolerated by the RS-25 servoactuator is roughly one octave, between about 6 Hz and 12 Hz. In the absence of friction, variations in this range produce a relatively small change in the transient performance characteristics. However, the coupling of gimbal bearing friction and the load compliance is significant. These effects are discussed in more detail in the companion papers.[6,8]

In order to determine the appropriate cutoff frequency, a convergence study was implemented as part of the MASV workflow. The results of a typical convergence analysis are shown in Figure 6, shown here for the Green Run hot fire configuration. The load stiffness as computed by MASV is in family with values computed using other finite element analysis techniques.[‡] Although the backup structure is slightly different for adjacent actuator degrees of freedom, the effective load stiffness is approximately the same for all gimbal DoF. As discussed in Refs.[6,8] the as-tested value was significantly lower in the non-firing condition, in part due to compliance in the gimbal bearing and small-amplitude nonlinearities associated with the actuator and structure. Subsequent frequency identification during hot fire showed that the thrusting condition stiffness was closer to the value predicted by the finite element model with propellant pressurization and cryo loading effects, and the remaining increase in the apparent load resonance frequency could be accounted for by the interplay of friction, mechanical deadbands, nonlinear load response, and gimbal bearing elasticity.[5,7,8]

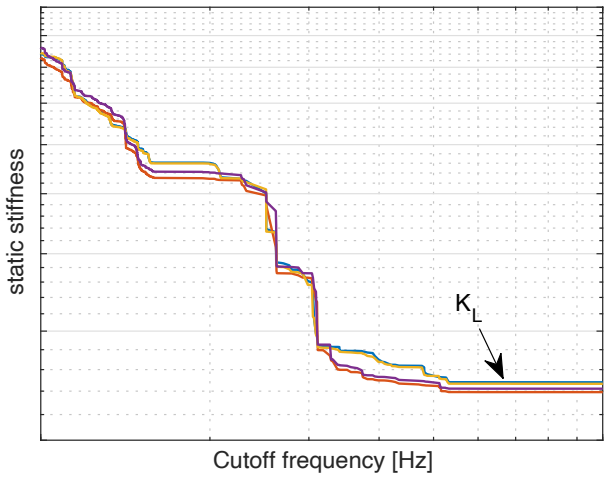

Figure 6. Computation of K_s as a function of modal frequency

Finally, MASV was used to produce both the closed-loop engine transient response and actuator piston transfer functions, to compare with those data as telemetered during test using string potentiometer and piston position feedback measurements (Figure 7). Piston position is the primary measure of the frequency of the load (anti)resonance,[6] and while engine position information was not available during the first flight of Artemis I, the correlated models incorporate system identification data and are used to predict the flight performance.[8] Here, the closed-loop piston antiresonance (notch) frequency appears close to 9.5 Hz, which is consistent with the MASV predictions for the flight configuration.

[‡]The reader is cautioned that depending on the technique, direct querying of a FEM can produce misleading results in

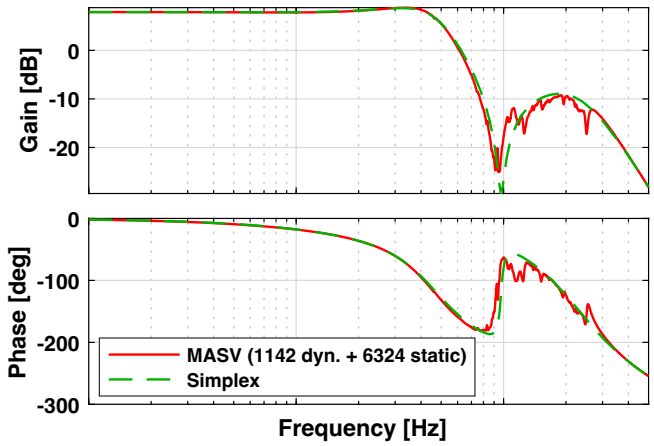

Figure 7. RS-25 actuator piston transfer function, GRHF configuration

6 CONCLUSIONS

In certain highly-coupled thrust vector control systems, and especially those used for vectoring of multiple liquid engines, it may be necessary to capture dynamic effects that span a wide spectrum of local and global structural modes. The present approach provides an analysis framework for incorporating potentially thousands of modes into a fully-coupled, multi-actuator simulation. Importantly, MASV and related formulations can be used to elucidate effects from a finite element model representation of the thrust structure that are not immediately obvious considering only the structural dynamics or the actuator dynamics alone.

The simplex formation, where the engine load response is approximated by a rigid inertia and a spring, is a reliable design tool for flight control performance and stability analysis unless friction or gimbal elasticity cannot be represented in a single plane.[5] However, it is important to consider that these simplified design models should be verified using a higher-fidelity approach to ensure that no adverse coupling can occur. Design models should be anchored to hot fire test data, especially when any or all of the components do not have a validated modeling pedigree in the flight configuration.

ACKNOWLEDGEMENTS

The authors would like to thank Carl Leake, Abhi Jain, and Arash Kalantari of JPL as well as Ivan Bertaska (MSFC) and Jeff Brouwer (Troy 7, Inc.) for their assistance in verifying the MASV implementation using DARTS. This work was supported by the NASA Marshall Space Flight Center under contract number 80MSFC18C0011.

determining the TVC load stiffness.

REFERENCES

[1] Jain, A., "DARTS - Multibody Modeling, Simulation and Analysis Software", 2019 Multibody Dynamics, ed. Andrés Kecskeméthy, Francisco Geu Flores, Springer, 2019.

[2] Schutte, et al., "Development and Verification of a Pipeline for Modeling Flexible Multibody Dynamics", NESC Technical Memo, NASA/TM−2020-5008164, NESC-RP-18-01312, August 2020.

[3] Stuart, B., et al., "Overview of the SLS Core Stage Thrust Vector Control System Design," AAS 23-152, American Astronautical Society Guidance, Navigation, and Control Conference, February 2023.

[4] Stuart, B., et al., "Core Stage TVC Systems Engineering Challenges in Reusing Heritage Hardware," AAS 23-154, American Astronautical Society Guidance, Navigation, and Control Conference, February 2023.

[5] Russell, C., et al., "Gimbal Bearing Friction in the SLS Core Stage Thrust Vector Control System," AAS 23-155, American Astronautical Society Guidance, Navigation, and Control Conference, February 2023.

[6] Wall, J., et al., "Design, Instrumentation, and Data Analysis for the SLS Core Stage Green Run Test Series," AAS 23-156, American Astronautical Society Guidance, Navigation, and Control Conference, February 2023.

[7] Moore, R., et al., "Structural Dynamics Observations in Space Launch System Green Run Hot Fire Testing," AAS 23-157, American Astronautical Society Guidance, Navigation, and Control Conference, February 2023.

[8] Wall, J., et al., "Flight Performance and Stability of Space Launch System Core Stage Thrust Vector Control," AAS 23-158, American Astronautical Society Guidance, Navigation, and Control Conference, February 2023.

[9] Orr, J., Wall, J., and Barrows, T., "Simulation-Based Analysis and Prediction of Thrust Vector Servoelastic Coupling," AAS 20-091, American Astronautical Society Guidance, Navigation, and Control Conference, February 2020.

[10] Thompson, Z., and Hung, J.C., "A Mathematical Model for a Space Vehicle Thrust Vector Control System," Scientific Report no. 15, Control Theory Group, University of Tennessee, August 24, 1967.